Mitsui *et al.*
Progress in Earth and Planetary Science (2024) 11:33
https://doi.org/10.1186/s40645-024-00638-7

Progress in Earth and Planetary Science

RESEARCH ARTICLE

Open Access

Quantifying the expansion rates of aftershock zones for magnitude-7 class earthquakes around the Japanese archipelago

Yuta Mitsui[1*], Yuya Utagawa[2] and Ayaka Miyamoto[3]

Abstract

Earthquakes (mainshocks) trigger sequences of aftershocks, the frequency of which diminishes following a power-law decay, while the spatial domain of these aftershocks extends logarithmically over time. The delineation of the aftershock zone can be modulated by variables beyond the magnitude of the mainshock, encompassing the location of the fault (whether the fault is at a plate boundary), the depth at which the event occurs, and the prevailing local stress conditions. Here, we evaluate the expansion rate of aftershock zones by analyzing earthquakes of magnitude-7 class in the vicinity of the Japanese archipelago. Prior studies have offered approximate assessments of expansion rates; however, our approach involves the utilization of a straightforward algorithm for the automated estimation of this metric, facilitating the compilation of a catalog. Across the dataset, no pronounced correlations were discerned between the expansion rate and other examined parameters. Yet, an inverse relationship is identified between the expansion rate and the b value of aftershocks for mainshocks occurring at plate boundaries. This observation suggests that the expansion rate of aftershock zones predominantly mirrors the stress field following the mainshock. Such a pattern is not detected in mainshocks occurring within the plate's interior. While the expansion rate of aftershock zones is likely influenced by various factors, aftershock zones may expand more rapidly with higher differential stress in areas surrounding hypocenters of major interplate earthquakes of magnitude 8 or 9.

Keywords Aftershocks, Expansion rates, Seismic b value, Interplate earthquakes, Intraplate earthquakes, Stress condition

1 Introduction

When an earthquake (mainshock) transpires, significant forces are exerted on the adjacent regions, leading to the occurrence of aftershocks. Initially, the force emanating from the mainshock is disseminated to the surrounding area through both dynamic and static stress changes (King et al. 1994; Felzer and Brodsky 2006; Toda et al. 2012). It is well established that the magnitude of the mainshock is directly proportional to the extent of the aftershock region (Tajima and Kanamori 1985; Yamanaka and Shimazaki 1990). Subsequently, processes that are delayed in time prompt alterations in the locations of aftershocks. Instances of such processes include postseismic deformation subsequent to the mainshock (Matsuzawa et al. 2004; Perfettini and Avouac 2004; Hsu et al. 2006) or the localized diminution of rock strength facilitated by pore fluids (Nur and Booker 1972; Yukutake and Iio 2017; Miller 2020), both of which can engender aftershocks. The spatial domain of aftershocks undergoes expansion over time (Chatelain et al. 1983; Henry and

*Correspondence:
Yuta Mitsui
mit@shizuoka.ac.jp
[1] Department of Geosciences, Shizuoka University, Shizuoka 422-8529, Japan
[2] Formerly at Department of Geosciences, Shizuoka University, Shizuoka 422-8529, Japan
[3] Formerly at Graduate School of Science and Technology, Shizuoka University, Shizuoka 422-8529, Japan

Das 2001), accompanied by a power-law decay in the frequency of aftershocks (Omori 1894; Utsu 1961).

The expansion rate of the aftershock zone is subject to influence by various factors, including the location of the fault (whether the fault is at a plate boundary), ambient temperature and pressure conditions, and local stress conditions. Nonetheless, a consensus has emerged in recent years around the general characteristic that expansion is proportional to the logarithm of time (Peng and Zhao 2009; Kato and Obara 2014; Hainzl et al. 2016; Ross et al. 2017). An underlying physical mechanism that shows promise is the concept that the aseismic afterslip following the mainshock serves as an effective trigger for aftershocks (Wesson 1987; Kato 2007; Ariyoshi et al. 2019). Beyond the afterslip, various transient (viscous) phenomena, such as power-law creep, are posited to play a critical role immediately following megathrust earthquakes (Agata et al. 2019; Morikami and Mitsui 2020). Independent of the presence of afterslip or other transient mechanisms, the aftershock zone is anticipated to undergo expansion to a certain degree as a result of a sequential occurrence of aftershocks (Helmstetter and Sornette 2002; Ozawa and Ando 2021). As mentioned above, a variety of cases have been reported and models have been proposed. However, there remains a notable scarcity of research that examines and compares actual seismicity in a comprehensive manner.

In this study, we examine the expansion rate of the aftershock zone and its determinants by analyzing magnitude-7 class earthquakes occurring in the vicinity of the Japanese archipelago, an area characterized by its advanced seismic observation networks. Initially, we perform an objective estimation of the aftershock zone expansion rate and compile a comprehensive catalog. Building on this groundwork, we proceed to investigate the controlling factors driving aftershock generation. Our exploration extends beyond the established characteristics of aftershocks, such as power-law decay and logarithmic spatial expansion, aiming to uncover new insights into the complex natural systems that govern seismic events.

2 Data

We utilize hypocenter catalog data from the Japan Meteorological Agency (JMA), selectively incorporating only those entries flagged with "high precision" in hypocenter determination. Our dataset comprises earthquakes of JMA magnitude 2.0 or greater, occurring within the timeframe of 2000–2021. During this period, major interplate earthquakes of magnitude 9 (the Tohoku earthquake in 2011) and magnitude 8 (the Tokachi-oki earthquake in 2003) occurred; however, due to the vastly different scale of aftershock activity associated with these events compared to smaller earthquakes, they are not categorized as "mainshocks" in this study. Additionally, aftershocks occurring within one day of these events are also excluded from being classified as "mainshocks." Among the remaining earthquakes, the largest recorded a magnitude of 7.4.

Earthquakes with JMA magnitudes ranging from 7.4 to 6.9, occurring around the Japanese archipelago between 2000 and 2021, are identified as potential "mainshocks" for the analysis of the aftershock zone expansion rate. From the perspective of balancing sufficient signal strength and a substantial population size, this study focuses on earthquakes down to a magnitude of 6.9. In this context, earthquakes in the vicinity of the Japanese archipelago can be categorized into subduction interplate earthquakes, which exhibit low-angle reverse faulting akin to the angle of the subducting oceanic plate, and intraplate earthquakes, including inland and intraslab events, as delineated by the centroid moment tensors (refer to Supplementary Table S1). In our categorization, we also refer to isobaths of the subducting plate and earthquake reports from the Headquarters for Earthquake Research Promotion. Due to the inferior quality (significant estimation errors) of the hypocenter catalog data, outer-rise earthquakes, which occur at a considerable distance from the seismic networks, are excluded from our study.

Consequently, we designate the 25 earthquakes depicted in Fig. 1 and Table 1 as "mainshocks." Among these, the magnitude 7.3 earthquake in 2011, cataloged as mainshock number 14 in Table 1, demands particular examination. Occurring approximately 2 days before the magnitude 9.0 Tohoku earthquake, this event is posited as a potential foreshock to the latter, more significant seismic occurrence (Hirose et al. 2011). In light of this, our analysis is confined to the examination of aftershocks that occurred prior to the Tohoku earthquake, with the aim of avoiding the influence of aftershock activity associated with the magnitude 9 event. In Table 1, mainshock numbers 3 and 4, with magnitudes of 7.1 and 7.4 respectively, occurred in close proximity to each other within 1 day, and their aftershock zones overlap (Park and Mori 2005). In our analysis for this study, both events are utilized; however, readers conducting their own analyses may consider excluding one of the two to avoid potential confounding effects due to the overlapping aftershock zones. In the case of the Kumamoto earthquake (magnitude 7.3) in 2016 (identified as mainshock number 22 in Table 1), prior in-depth studies (e.g., Uchide et al. 2016; Yagi et al. 2016) have documented the active dynamic triggering of distant earthquakes at locales unassociated with the fault of the mainshock. This paper treats it similarly to other

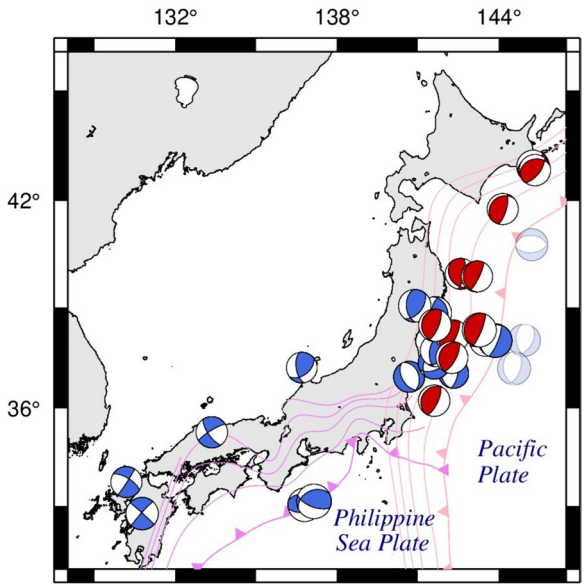

Fig. 1 Magnitude-7 class "mainshocks" around the Japanese archipelago. The beachballs display the double couple part of the centroid moment tensors estimated by JMA. Interplate and intraplate earthquakes, which can be determined from the centroid moment tensors (Supplementary Table S1), are shown in red and blue. The vague gray beachballs show the outer-rise earthquakes, which were excluded from our study. The light pink lines depict the trench and the isobaths of the subducting Pacific Plate, plotted at 20-km intervals up to a depth of 80 km (Iwasaki et al. 2015; Lindquist et al. 2004). The violet lines represent those of the subducting Philippine Sea Plate

mainshocks, yet a cautious approach may be warranted when discussing it in detail.

We investigate the spatiotemporal dynamics of aftershocks, defined as earthquakes occurring in proximity to a "mainshock." Despite the spatial diversity observed in aftershock distributions, we utilize the three-dimensional distance from the "mainshock" hypocenter as an isotropic spatial coordinate to enable a cohesive analysis. This approach facilitates a standardized discussion across different seismic events. The spatiotemporal definition of aftershocks is not straightforward. In this study, we initially conduct our analysis using definition commonly employed in existing research. Subsequently, we also evaluate the implications of slightly altering the definition.

3 Methods

3.1 Estimation of the expansion rate of aftershock zone

The expansion rate of the aftershock zone has traditionally been deduced from hypocenter data through visual inspection. However, in the present study, this rate is quantitatively estimated through a regression analysis, incorporating two variables: the logarithm of the elapsed time since the mainshock and the three-dimensional (hypocentral) distance from the mainshock hypocenter.

The definition of the aftershock zone is conducted in accordance with the well-established methodology in previous studies (Gardner and Knopoff 1974; van Stiphout et al. 2012). Specifically, the temporal window of the range is defined by the elapsed time t [days] since the mainshock, and the spatial window is defined by the distance d [km] from the hypocenter of the mainshock, as delineated by the following equation:

$$t = 10^{0.032M+2.7389} \tag{1}$$

$$d = 10^{0.1238M+0.983} \tag{2}$$

where M is the magnitude of the mainshock. In defining the aftershock zones for the 25 mainshocks examined in this study, the temporal parameter t is set between 911.4 and 945.6 days, and the spatial parameter d ranges from 68.7 to 79.3 km. Moreover, in light of the proximity between certain mainshocks (Table 1), the implications of utilizing shorter temporal interval (t) will be examined.

Figure 2 presents an illustration of the expansion of the aftershock zone and the calculation of the expansion rate for the mainshock numbered 10 in Table 1, namely the 2008 off Ibaraki earthquake (Kubo and Nishikawa 2020). Within Fig. 2a–d, it is evident that the aftershock zone expands over time. To quantify this expansion rate, a scatterplot depicting the logarithm of elapsed time versus the hypocentral distance (Fig. 2e) is utilized, followed by a simple linear regression analysis of the points along the outer boundary. The regression analysis focuses on aftershocks at the greatest hypocentral distances as time progresses. It is important to note that the points defining the outer boundary are determined based on the spatiotemporal distribution of the aftershock hypocenters, without the imposition of any artificial time window for their selection. We present more information for all the 25 mainshocks, in Supplementary Data S1.

3.2 Estimation of Gutenberg–Richter b value

We focus on the Gutenberg–Richter b value (Gutenberg and Richter 1944) as a potential indicator of local stress associated with the expansion of the aftershock zone. The Gutenberg-Richter law posits that, for any given magnitude M, the number of earthquakes exceeding this magnitude, denoted as N, adheres to the expression $\log_{10} N \propto -bM$. This b value demonstrates a tendency to negatively correlate with differential stress (Scholz 1968; Wyss 1973), and has been extensively employed in the research about the stress conditions on faults (Schorlemmer et al. 2005; Nanjo et al. 2012; Spada et al. 2013; Chiba 2020).

Table 1 Magnitude-7 class "mainshocks" around the Japanese archipelago in this study

	Date (JST)	Longitude, latitude [deg.]	Depth [km]	Magnitude	Type
1	October 6, 2000	133.349, 35.274	8.96	7.3	Intra
2	May 26, 2003	141.651, 38.821	72.03	7.1	Intra
3	September 5, 2004	136.798, 33.033	37.58	7.1	Intra
4	September 5, 2004	137.141, 33.138	43.54	7.4	Intra
5	November 29, 2004	145.276, 42.946	48.17	7.1	Inter
6	December 6, 2004	145.343, 42.848	45.84	6.9	Inter
7	March 20, 2005	130.176, 33.739	9.24	7.0	Intra
8	August 16, 2005	142.278, 38.150	42.04	7.2	Inter
9	March 25, 2007	136.686, 37.221	10.70	6.9	Intra
10	May 8, 2008	141.608, 36.228	50.57	7.0	Inter
11	June 14, 2008	140.881, 39.030	7.77	7.2	Intra
12	July 19, 2008	142.265, 37.521	31.55	6.9	Inter
13	September 11, 2008	144.152, 41.776	30.86	7.1	Inter
14	March 9, 2011	143.280, 38.329	8.28	7.3	Inter
15	April 7, 2011	141.920, 38.204	65.89	7.2	Intra
16	April 11, 2011	140.673, 36.946	6.42	7.0	Intra
17	June 23, 2011	142.591, 39.948	36.40	6.9	Inter
18	July 10, 2011	143.507, 38.032	34.00	7.3	Intra
19	December 7, 2012	143.867, 38.020	49.00	7.3	Intra
20	July 12, 2014	142.321, 37.050	33.00	7.0	Intra
21	February 17, 2015	143.193, 39.872	12.72	6.9	Inter
22	April 16, 2016	130.763, 32.755	12.45	7.3	Intra
23	November 22, 2016	141.604, 37.355	24.50	7.4	Intra
24	February 13, 2021	141.699, 37.729	55.38	7.3	Intra
25	March 20, 2021	141.628, 38.468	59.46	6.9	Inter

The longitude, latitude, and depth of hypocenters and the magnitude are based on the earthquake catalog provided by JMA. The type of earthquakes, interplate ("inter") or intraplate ("intra"), is determined from the centroid moment tensors estimated by JMA

Addressing the magnitude completeness problem in earthquake catalogs (e.g., Ogata and Katsura 1993; Nanjo et al. 2010; Mignan 2012), the recent development of the b-positive method (van der Elst 2021) marks a significant advancement in accurately estimating b values. The original Gutenberg–Richter law can be expressed as a probability density function for earthquakes exceeding a threshold magnitude M_c, which is influenced by the conditions of seismic observation, as follows:

$$f(x) = \beta \exp(-\beta x) \quad \text{for } x \geq 0 \tag{3}$$

where $x = M - M_c$ and $\beta = b\ln(10)$. M_c is generally not uniform across space and time; for instance, early aftershocks tend to be obscured by overlapping seismic waves (Kato et al. 2012; Omi et al. 2013; Sawazaki and Enescu 2014). The b-positive method (van der Elst 2021) utilizes the difference in magnitude, denoted as M', rather than the absolute magnitudes. Namely, it employs the magnitude differences ($M' \geq 0.1$) between successive earthquakes where the magnitude of the second earthquake exceeds that of the first. This approach culminates in the following relationship:

$$f(M') = \beta \exp(-\beta M') \tag{4}$$

The b value for each aftershock sequence can be estimated based on the maximum likelihood method (Aki 1965), yielding the estimated b value as follows:

$$b = \frac{\log_{10}(e)}{\overline{M'} - 0.05} \tag{5}$$

where $\overline{M'}$ is the mean magnitude difference and 0.05 represents the resolution of the catalog (Guo and Ogata 1997). We present histograms of the magnitude differences for all the 25 mainshocks, in Supplementary Data S2. The 90% confidence interval is obtained through the analysis of 500 bootstrapping samples.

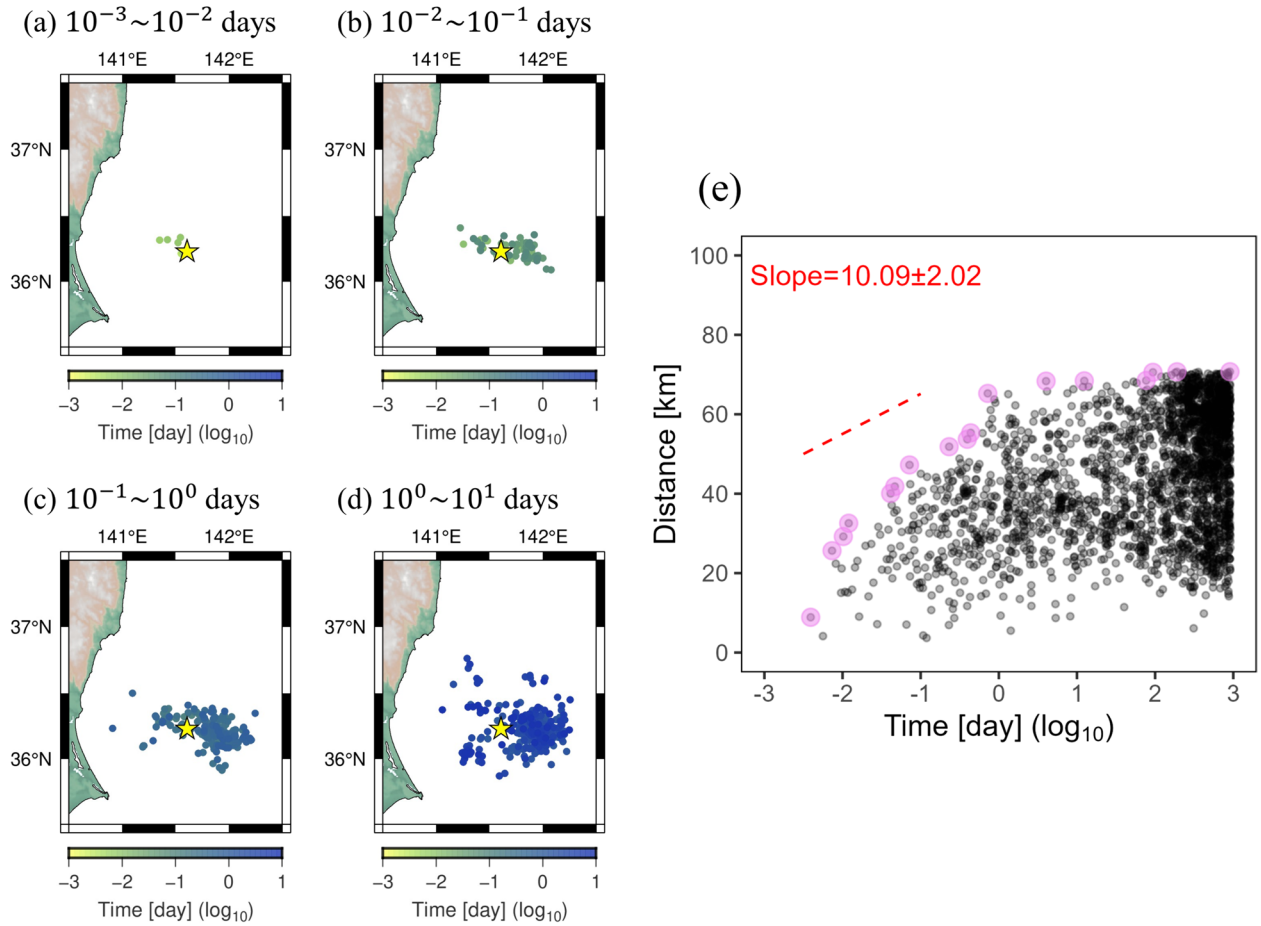

Fig. 2 Expansion of the aftershock zone and estimation of the expansion rate for the 2008 off Ibaraki interplate earthquake (magnitude 7.0). Panels **a**–**d** show the spatiotemporal distribution of the aftershocks by elapsed time from the mainshock. Panel **e** exhibits the scatterplot of the logarithm of the elapsed time versus the hypocentral distance. The pink circles denote the temporal progression of the locations of aftershocks at the greatest hypocentral distances (outer boundary). The slope of the dashed red line represents the estimated expansion rate of the aftershock zone, whereas the range of error is indicative of the 90% confidence interval

4 Results

Figure 3 and Table 2 present the estimated expansion rates of the aftershock zones for the 25 magnitude-7 class mainshocks, as depicted in Fig. 1 and Table 1. The spatial distribution and the triangle diagram of focal mechanisms (Frohlich 1992), as illustrated in Fig. 3, do not reveal any discernible patterns in the expansion rates of aftershock zones. Nonetheless, from a physical perspective, it is plausible to conjecture that the occurrence of aftershocks may be influenced by factors such as the location of the fault (whether the fault is at a plate boundary), the ambient temperature and pressure conditions, or the local stress conditions. Consequently, we undertake a statistical examination of these aspects.

Initially, we examine the presence of significant disparities in the expansion rates of aftershock zones between interplate and intraplate earthquakes, as delineated in Table 1. The average expansion rate for interplate earthquakes is determined to be 12.46 [km/decade], in contrast to 12.79 [km/decade] for intraplate earthquakes, with "decade" in this context referring to a single digit in the base-10 logarithm. No significant difference exists between the two types of earthquakes.

Subsequently, we shift our attention to the focal depth of the mainshock as a parameter approximately indicative of the ambient temperature and pressure conditions, and investigate its correlation with the expansion rate of the aftershock zones. The correlation coefficient is calculated to be − 0.28, implying that the depth at which the event occurs does not exert a controlling influence on the expansion of aftershock zones.

Finally, we establish a correlation between the seismic b value of the aftershocks (Table 2), as an indicator of local differential stress (Scholz 1968, 2015), and the expansion rate of the aftershock zones, depicted in

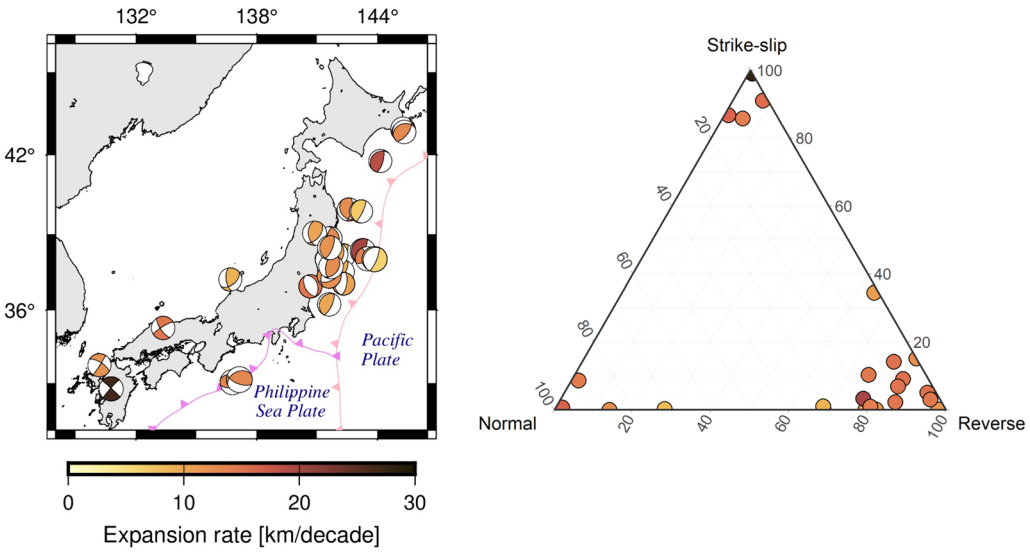

Fig. 3 Estimated aftershock zone expansion rates for the magnitude-7 class mainshocks (Fig. 1). The left figure represents the spatial distribution, while the right figure shows the triangle diagram of focal mechanisms (Frohlich 1992), to demonstrate the estimated expansion rates

Fig. 4. The correlation coefficient is -0.19, indicating no significant correlation.

However, in Fig. 4, when distinguishing between mainshocks of interplate earthquakes and those of intraplate earthquakes, a certain characteristic becomes apparent. Namely, when isolating only the interplate earthquakes, a clear negative correlation is observed between the expansion rate of the aftershock zones and the b value. The correlation coefficient was found to be −0.75, with a p value of 0.01. Mainshocks No. 13 and No. 14 hold significant importance. This negative correlation implies a positive correlation between the aftershock expansion rate and local stress after the mainshock, because the b value is negatively correlated with local differential stress (Schorlemmer et al. 2005; Nishikawa and Ide 2014; Scholz 2015). It would be mechanically plausible when considering the simpler aftershock propagation along the plane-like mature faults at plate boundaries. Additionally, aseismic afterslip or other transient mechanisms mentioned in the introduction section might contribute to this simpler propagation pattern.

In the relationship between the aftershock expansion rate and the b value for interplate earthquakes (Fig. 4), mainshocks No. 13 and No. 14 are characterized by their high expansion rates and low b values. Notably, the hypocenters of these mainshocks are located in close proximity to the larger magnitude 8 and 9 earthquakes, compared to other mainshocks, suggesting significant implications. For example, the 2008 event (No. 13) at longitude 144.152°, latitude 41.776°, depth 30.86 km, was near the magnitude 8.0 2003 Tokachi-oki earthquake (longitude 144.079°, latitude 41.779°, depth 45.07 km), and the 2011 event (No. 14), at longitude 143.280°, latitude 38.329°, depth 8.28 km, occurred near the magnitude 9.0 2011 Tohoku-oki earthquake (longitude 142.861°, latitude 38.104°, depth 23.74 km), potentially serving as a foreshock, as previously mentioned. This implies that the areas surrounding the hypocenters of major earthquakes of magnitude 8 or 9 tend to have higher differential stress compared to other areas. Such an effect is less apparent in the intraplate mainshocks, where their focal mechanisms and the plate boundary slip substantially differ.

The persistence of high stress in the area surrounding the hypocenter 5 years after the magnitude 8.0 2003 Tokachi-oki earthquake aligns with a previous study, suggesting that the stress release of this earthquake did not significantly alter the stress field (Tormann et al. 2015). Although numerous cases have been documented where b values increase in surrounding areas following large earthquakes (Gulia and Wiemer 2019), the 2003 Tokachi-oki earthquake appears not to conform to this pattern. To further explore this issue, additional investigation might be warranted using statistical models such as the epidemic-type aftershock sequence (ETAS) model, properly defining background seismicity distinct from aftershocks (Ueda and Kato 2023).

5 Discussion

We examine the definition of the aftershock zone that has been established (Gardner and Knopoff 1974; van Stiphout et al. 2012). Given the high background seismicity surrounding the Japanese archipelago, the current definition of the time window (ranging from t =

Table 2 Estimated parameters for each mainshock (Table 1)

	Expansion rate [km/decade]	b value (aftershock)
1	14.61 ± 2.08	0.954 ± 0.049
2	12.88 ± 1.86	0.797 ± 0.032
3[a]	13.37 ± 2.84	0.827 ± 0.037
4[a]	13.14 ± 1.84	0.846 ± 0.040
5	13.37 ± 1.47	0.669 ± 0.042
6	13.04 ± 1.53	0.675 ± 0.050
7	12.14 ± 3.19	0.868 ± 0.052
8	8.65 ± 1.95	0.735 ± 0.046
9	9.06 ± 1.41	0.856 ± 0.038
10	10.09 ± 2.02	0.839 ± 0.042
11	10.39 ± 2.04	0.908 ± 0.037
12	9.17 ± 2.01	0.796 ± 0.044
13	18.62 ± 1.56	0.527 ± 0.049
14[b]	20.07 ± 4.91	0.481 ± 0.055
15	9.61 ± 3.98	0.761 ± 0.014
16	14.66 ± 2.55	0.808 ± 0.014
17	12.67 ± 2.40	0.658 ± 0.028
18	13.74 ± 1.73	0.829 ± 0.029
19	6.10 ± 2.55	0.875 ± 0.034
20	10.47 ± 2.25	0.853 ± 0.030
21	6.83 ± 1.82	0.630 ± 0.041
22[c]	26.81 ± 8.74	0.892 ± 0.027
23	12.23 ± 1.96	0.841 ± 0.020
24[d]	12.61 ± 3.23	0.838 ± 0.027
25[d]	12.08 ± 3.18	0.746 ± 0.058

[a] In proximity to each other within one day with overlapped aftershock zones

[b] With only aftershocks up to about two days before the magnitude 9 Tohoku earthquake in 2011

[c] With active dynamic triggering of distant earthquakes

[d] With only aftershocks up to the end of 2021 (due to catalog limitation)

The expansion rate is derived from the regression analysis on the logarithm of the elapsed time and the hypocentral distance. The b value (aftershocks) represents the b-positive estimation results for aftershocks. The error ranges represent the 90% confidence intervals

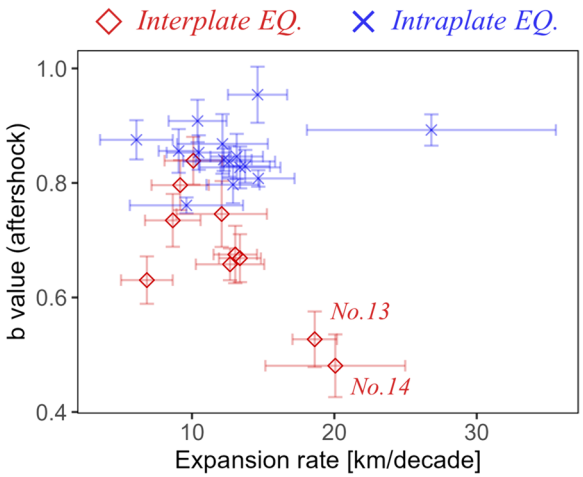

Fig. 4 Scatterplot of the aftershock zone expansion rate versus the seismic b value of the aftershocks. The range of error is indicative of the 90% confidence interval

911.4 to 945.6 days) from Eq. (1) does not preclude the possibility of incorporating earthquakes unrelated to aftershock activity within this timeframe.

Taking into account the results obtained thus far (Supplementary Data S1), where the time parameter ranged from t = 911.4 to 945.6 days, we modified this parameter to t = 10 days in order to conduct an analysis focused exclusively on the early aftershocks. The duration of 10 days corresponds to an order of magnitude greater than the one-day period previously examined as early aftershocks in previous studies (Omi et al. 2013, 2014).

Figure 5 presents a comparison between the estimated results of aftershock zone expansion rates and b values with the time parameter set to t = 10 days and the results from the original time parameters. The correlation coefficients are sufficiently high at 0.71 and 0.95, respectively, indicating that the estimated values do not significantly change even when the time parameter t is altered by two orders of magnitude. Supplementary Data S3 and S4 show results analogous to those in Supplementary Data S1 and S2, with the time parameter t adjusted to 10 days.

We examine the correlation with the various parameters upon adjusting the time parameter to t = 10 days. Despite the two orders of magnitude change in the value of t, there are no fundamental changes to the findings discussed in the results section; no significant correlation is observed between the aftershock zone expansion rate and either the depth of the mainshock or b value. When the analysis is limited to the interplate earthquakes, the correlation coefficient between the aftershock zone expansion rate and b value slightly decreases to -0.60 (from -0.75), which is still meaningful.

Furthermore, we address the results obtained when using another scaling relations (Uhrhammer 1986) that involve t [days] and d [km], which are different from those in Eqs. (1) and (2), in the definition of aftershocks. The equations are given by:

$$t = \exp(1.235M - 2.87) \tag{6}$$

$$d = \exp(0.804M - 1.024) \tag{7}$$

For the 25 mainshocks in this study, the temporal parameter t is set between 284.7 and 527.9 days, and the spatial parameter d ranges from 92.2 km to 137.8 km. Supplementary Table S3 compiles the results for the

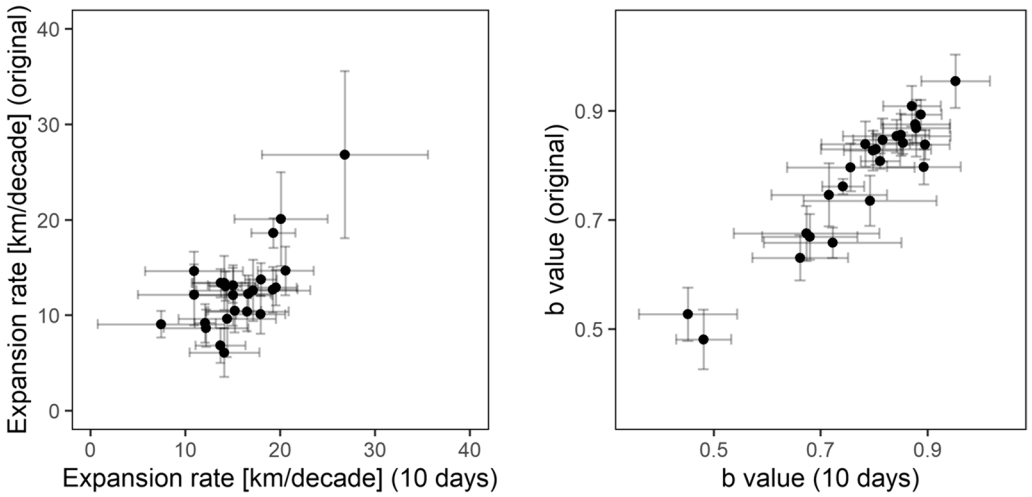

Fig. 5 A comparison between the estimated results of aftershock zone expansion rates and b values with the time parameter set to t = 10 days and the results from the original time parameters. The left figure displays the results for the aftershock zone expansion rates (correlation coefficient = 0.71), while the right figure represents the outcomes for the b values (correlation coefficient = 0.95). The range of error is indicative of the 90% confidence interval

aftershock zone expansion rates and the b values. The values of the aftershock zone expansion rates tend to increase compared to the original results (Table 2), yet there are no fundamental changes to the findings. When focusing solely on interplate earthquakes, the correlation coefficient between the aftershock zone expansion rate and the b value stands at −0.79.

Finally, we check the impact of the method used to estimate the b value. We have estimated the b value using Eq. (5), which means that it has been estimated within the range of $M\prime \geq 0.1$. The previous study (van der Elst 2021) recommended verifying a minimum magnitude difference greater than 0.1; therefore, we attempt to estimate the b value at $M\prime \geq 0.2$. As a result, the estimated b values differed by a maximum of 0.04 and less than 0.01 in more than half of the mainshocks compared to the original values (Table 2). Therefore, this point does not affect the main conclusions of this paper.

While there is ongoing potential for refinement in our methodology for individual mainshocks, we propose that we have effectively discerned shared characteristics among aftershocks through the utilization of a straightforward approach.

6 Conclusions

We conducted a systematic investigation into the expansion rates, measured in logarithmic time, of aftershock zones associated with 25 mainshocks of magnitude-7 class (Mj 7.4–6.9) occurring in the vicinity of the Japanese archipelago. When limited to interplate earthquakes, a negative correlation was observed between the expansion rate of the aftershock zones and the b value of the aftershocks. This reflects a tendency for aftershock zones to expand more rapidly in areas with higher differential stress, such as areas surrounding the hypocenters of major interplate earthquakes of magnitude 8 or 9.

Abbreviation

JMA Japan meteorological agency

Supplementary Information

The online version contains supplementary material available at https://doi.org/10.1186/s40645-024-00638-7.

Additional file 1
Additional file 2
Additional file 3
Additional file 4
Additional file 5
Additional file 6
Additional file 7

Acknowledgements

We thank the Japan Meteorological Agency for providing the earthquake data. The plate models by Iwasaki et al. (2015) were constructed from topography and bathymetry data by Geospatial Information Authority of Japan (250-m digital map), Japan Oceanographic Data Center (500m mesh bathymetry data, J-EGG500, http://www.jodc.go.jp/jodcweb/JDOSS/infoJEGG_j.html) and Geographic Information Network of Alaska, University of Alaska (Lindquist et al., 2004). We are grateful to Taku Ueda, Futoshi Yamashita, and Aitaro Kato for fruitful comments and discussions. We appreciate two anonymous reviewers for their insightful comments and suggestions, which have greatly improved the manuscript.

Author contributions
YM conceived the study, verified the whole results, and drafted the manuscript. YU analyzed the data. AM developed the computer programs. All authors contributed to the manuscript.

Funding
This study is funded by Japan Society for the Promotion of Science KAKENHI Grant 22H00176.

Availability of data and material
The datasets supporting the conclusions of this article are included within the article and its additional files. The hypocenter catalog and centroid moment tensor catalog used in this study are available from JMA [http://www.data.jma.go.jp/svd/eqev/data/bulletin/index_e.html]. The earthquake reports can be accessed through the Headquarters for Earthquake Research Promotion [https://www.jishin.go.jp/main/chousa/chousa-e.htm].

Declarations

Competing interests
The authors declare that they have no competing interest.

Received: 29 February 2024 Accepted: 7 June 2024
Published online: 16 June 2024

References

Agata R, Barbot SD, Fujita K et al (2019) Rapid mantle flow with power-law creep explains deformation after the 2011 Tohoku mega-quake. Nat Comm 10:1385. https://doi.org/10.1038/s41467-019-08984-7
Aki K (1965) Maximum likelihood estimate of b in the formula logN=a-bM and its confidence limits. Bull Earthq Res Inst 43:237–239
Ariyoshi K, Ampuero J-P, Bürgmann R et al (2019) Quantitative relationship between aseismic slip propagation speed and frictional properties. Tectonophysics 767:128151. https://doi.org/10.1016/j.tecto.2019.06.021
Chatelain J-L, Cardwell RK, Isacks BL (1983) Expansion of the aftershock zone following the Vanuatu (New Hebrides) Earthquake on 15 July 1981. Geophys Res Lett 10:385–388. https://doi.org/10.1029/GL010i005p00385
Chiba K (2020) Stress state along the western Nankai Trough subduction zone inferred from b-values, long-term slow-slip events, and low-frequency earthquakes. Earth Planets Space 72:3. https://doi.org/10.1186/s40623-020-1130-7
Felzer KR, Brodsky EE (2006) Decay of aftershock density with distance indicates triggering by dynamic stress. Nature 441:735–738. https://doi.org/10.1038/nature04799
Frohlich C (1992) Triangle diagrams: ternary graphs to display similarity and diversity of earthquake focal mechanisms. Phys Earth Planet Int 75:193–198. https://doi.org/10.1016/0031-9201(92)90130-N
Gardner JK, Knopoff L (1974) Is the sequence of earthquakes in Southern California, with aftershocks removed, Poissonian? Bull Seis Soc Am 64:1363–1367. https://doi.org/10.1785/BSSA0640051363
Gulia L, Wiemer S (2019) Real-time discrimination of earthquake foreshocks and aftershocks. Nature 574:193–199. https://doi.org/10.1038/s41586-019-1606-4
Guo Z, Ogata Y (1997) Statistical relations between the parameters of aftershocks in time, space, and magnitude. J Geophys Res 102:2857–2873. https://doi.org/10.1029/96JB02946
Gutenberg B, Richter CF (1944) Frequency of earthquakes in California. Bull Seis Soc Am 34:185–188
Hainzl S, Fischer T, Čermáková H et al (2016) Aftershocks triggered by fluid intrusion: evidence for the aftershock sequence occurred 2014 in West Bohemia/Vogtland. J Geophys Res 121:2575–2590. https://doi.org/10.1002/2015JB012582
Helmstetter A, Sornette D (2002) Diffusion of epicenters of earthquake aftershocks, Omori's law, and generalized continuous-time random walk models. Phys Rev E 66:061104. https://doi.org/10.1103/PhysRevE.66.061104
Henry C, Das S (2001) Aftershock zones of large shallow earthquakes: fault dimensions, aftershock area expansion and scaling relations. Geophys J Int 147:272–293. https://doi.org/10.1046/j.1365-246X.2001.00522.x
Hirose F, Miyaoka K, Hayashimoto N et al (2011) Outline of the 2011 off the Pacific coast of Tohoku Earthquake (Mw 9.0)-seismicity: foreshocks, mainshock, aftershocks, and induced activity. Earth Planets Sp 63:513–518. https://doi.org/10.5047/eps.2011.05.019
Hsu Y-J, Simons M, Avouac J-P et al (2006) Frictional afterslip following the 2005 Nias-Simeulue earthquake, Sumatra. Science 312:1921–1926. https://doi.org/10.1126/science.1126960
Iwasaki T, Sato H, Shinohara M, Ishiyama T, Hashima A (2015) Fundamental structure model of island arcs and subducted plates in and around Japan. In: AGU 2015 Fall Meeting, San Francisco. T31B-2878
Kato N (2007) Expansion of aftershock areas caused by propagating post-seismic sliding. Geophys J Int 168:797–808. https://doi.org/10.1111/j.1365-246X.2006.03255.x
Kato A, Obara K (2014) Step-like migration of early aftershocks following the 2007 Mw 6.7 Noto-Hanto earthquake, Japan. Geophys Res Lett 41:3864–3869. https://doi.org/10.1002/2014GL060427
Kato A, Obara K, Igarashi T et al (2012) Propagation of slow slip leading up to the 2011 M(w) 9.0 Tohoku-Oki earthquake. Science 335:705–708. https://doi.org/10.1126/science.1215141
King GCP, Stein RS, Lin J (1994) Static stress changes and the triggering of earthquakes. Bull Seis Soc Am 84:935–953
Kubo H, Nishikawa T (2020) Relationship of preseismic, coseismic, and postseismic fault ruptures of two large interplate aftershocks of the 2011 Tohoku earthquake with slow-earthquake activity. Sci Rep 10:12044. https://doi.org/10.1038/s41598-020-68692-x
Lindquist KG, Engle K, Stahlke D, Price E (2004) Global topography and bathymetry grid improves research efforts. Eos Trans AGU 85(19):186. https://doi.org/10.1029/2004EO190003
Matsuzawa T, Uchida N, Igarashi T et al (2004) Repeating earthquakes and quasi-static slip on the plate boundary east off northern Honshu, Japan. Earth Planets Space 56:803–811
Mignan A (2012) Functional shape of the earthquake frequency-magnitude distribution and completeness magnitude. J Geophys Res. https://doi.org/10.1029/2012JB009347
Miller SA (2020) Aftershocks are fluid-driven and decay rates controlled by permeability dynamics. Nat Commun 11:5787. https://doi.org/10.1038/s41467-020-19590-3
Morikami S, Mitsui Y (2020) Omori-like slow decay ($p < 1$) of postseismic displacement rates following the 2011 Tohoku megathrust earthquake. Earth Planets Space 72:37. https://doi.org/10.1186/s40623-020-01162-w
Nanjo KZ, Ishibe T, Tsuruoka H et al (2010) Analysis of the completeness magnitude and seismic network coverage of Japan. Bull Seis Soc Am 100:3261–3268. https://doi.org/10.1785/0120100077
Nanjo KZ, Hirata N, Obara K, Kasahara K (2012) Decade-scale decrease in b value prior to the M9-class 2011 Tohoku and 2004 Sumatra quakes. Geophys Res Lett. https://doi.org/10.1029/2012GL052997
Nishikawa T, Ide S (2014) Earthquake size distribution in subduction zones linked to slab buoyancy. Nat Geosci 7:904–908. https://doi.org/10.1038/ngeo2279
Nur A, Booker JR (1972) Aftershocks caused by pore fluid flow? Science 175:885–887. https://doi.org/10.1126/science.175.4024.885
Ogata Y, Katsura K (1993) Analysis of temporal and spatial heterogeneity of magnitude frequency distribution inferred from earthquake catalogues. Geophys J Int 113:727–738. https://doi.org/10.1111/j.1365-246X.1993.tb04663.x
Omi T, Ogata Y, Hirata Y, Aihara K (2013) Forecasting large aftershocks within one day after the main shock. Sci Rep. https://doi.org/10.1038/srep02218
Omi T, Ogata Y, Hirata Y, Aihara K (2014) Estimating the ETAS model from an early aftershock sequence. Geophys Res Lett 41:850–857. https://doi.org/10.1002/2013GL058958
Omori F (1894) On the aftershocks of earthquakes. J Coll Sci Imp Univ Tokyo 7:111–120
Ozawa S, Ando R (2021) Mainshock and aftershock sequence simulation in geometrically complex fault zones. J Geophys Res 126:e2020JB020865. https://doi.org/10.1029/2020JB020865

Park S-C, Mori J (2005) The 2004 sequence of triggered earthquakes off the Kii peninsula, Japan. Earth Planets Space 57:315–320. https://doi.org/10.1186/BF03352569
Peng Z, Zhao P (2009) Migration of early aftershocks following the 2004 Parkfield earthquake. Nat Geosci 2:877–881. https://doi.org/10.1038/ngeo697
Perfettini H, Avouac J-P (2004) Postseismic relaxation driven by brittle creep: a possible mechanism to reconcile geodetic measurements and the decay rate of aftershocks, application to the Chi-Chi earthquake, Taiwan. J Geophys Res. https://doi.org/10.1029/2003JB002488
Ross ZE, Rollins C, Cochran ES et al (2017) Aftershocks driven by afterslip and fluid pressure sweeping through a fault-fracture mesh. Geophys Res Lett 44:8260–8267. https://doi.org/10.1002/2017GL074634
Sawazaki K, Enescu B (2014) Imaging the high-frequency energy radiation process of a main shock and its early aftershock sequence: The case of the 2008 Iwate-Miyagi Nairiku earthquake, Japan. J Geophys Res 119:4729–4746. https://doi.org/10.1002/2013JB010539
Scholz CH (1968) The frequency-magnitude relation of microfracturing in rock and its relation to earthquakes. Bull Seis Soc Am 58:399–415. https://doi.org/10.1785/BSSA0580010399
Scholz CH (2015) On the stress dependence of the earthquake b-value. Geophys Res Lett 42:1399–1402. https://doi.org/10.1002/2014GL062863
Schorlemmer D, Wiemer S, Wyss M (2005) Variations in earthquake-size distribution across different stress regimes. Nature 437:539–542. https://doi.org/10.1038/nature04094
Spada M, Tormann T, Wiemer S, Enescu B (2013) Generic dependence of the frequency-size distribution of earthquakes on depth and its relation to the strength profile of the crust. Geophys Res Lett 40:709–714. https://doi.org/10.1029/2012GL054198
Tajima F, Kanamori H (1985) Global survey of aftershock area expansion patterns. Phys Earth Planet Int 40:77–134. https://doi.org/10.1016/0031-9201(85)90066-4
Toda S, Stein RS, Beroza GC, Marsan D (2012) Aftershocks halted by static stress shadows. Nat Geosci 5:410–413. https://doi.org/10.1038/ngeo1465
Tormann T, Enescu B, Woessner J, Wiemer S (2015) Randomness of megathrust earthquakes implied by rapid stress recovery after the Japan earthquake. Nat Geosci 8:152–158. https://doi.org/10.1038/ngeo2343
Uchide T, Horikawa H, Nakai M et al (2016) The 2016 Kumamoto-Oita earthquake sequence: aftershock seismicity gap and dynamic triggering in volcanic areas. Earth Planets Space. https://doi.org/10.1186/s40623-016-0556-4
Ueda T, Kato A (2023) Aftershocks following the 2011 Tohoku-Oki earthquake driven by both stress transfer and afterslip. Prog Earth Planet Sci 10:31. https://doi.org/10.1186/s40645-023-00564-0
Uhrhammer R (1986) Characteristics of northern and central California seismicity. Earthq Notes 57(1):21
Utsu T (1961) A statistical study on the occurrence of aftershocks. Geophys Mag 30:521–605
van der Elst NJ (2021) B-positive: a robust estimator of aftershock magnitude distribution in transiently incomplete catalogs. J Geophys Res 126:e2020JB021027. https://doi.org/10.1029/2020JB021027
van Stiphout T, Zhuang J, Marsan D (2012) Seismicity declustering. Commun Online Resour Stat Seism Anal. https://doi.org/10.5078/corssa-52382934
Wesson RL (1987) Modelling aftershock migration and afterslip of the San Juan Bautista, California, earthquake of October 3, 1972. Tectonophysics 144:215–229. https://doi.org/10.1016/0040-1951(87)90019-9
Wyss M (1973) Towards a physical understanding of the earthquake frequency distribution. Geophys J R Astr Soc 31:341–359. https://doi.org/10.1111/j.1365-246X.1973.tb06506.x
Yagi Y, Okuwaki R, Enescu B et al (2016) Rupture process of the 2016 Kumamoto earthquake in relation to the thermal structure around Aso volcano. Earth Planets Space. https://doi.org/10.1186/s40623-016-0492-3
Yamanaka Y, Shimazaki K (1990) Scaling relationship between the number of aftershocks and the size of the main shock. J Phys Earth 38:305–324
Yukutake Y, Iio Y (2017) Why do aftershocks occur? Relationship between mainshock rupture and aftershock sequence based on highly resolved hypocenter and focal mechanism distributions. Earth Planets Space. https://doi.org/10.1186/s40623-017-0650-2

Publisher's Note